Direct observation of multiple misfolding pathways in a single prion protein molecule

Hao Yu[a,1], Xia Liu[a,1], Krishna Neupane[a], Amar Nath Gupta[a], Angela M. Brigley[b], Allison Solanki[a], Iveta Sosova[b], and Michael T. Woodside[a,b,2]

[a]Department of Physics, University of Alberta, Edmonton AB, T6G 2G7 Canada; and [b]National Institute for Nanotechnology, National Research Council Canada, Edmonton AB, T6G 2M9 Canada

Edited by Stanley B. Prusiner, University of California, San Francisco, San Francisco, CA, and approved January 17, 2012 (received for review May 13, 2011)

Protein misfolding is a ubiquitous phenomenon associated with a wide range of diseases. Single-molecule approaches offer a powerful tool for deciphering the mechanisms of misfolding by measuring the conformational fluctuations of a protein with high sensitivity. We applied single-molecule force spectroscopy to observe directly the misfolding of the prion protein PrP, a protein notable for having an infectious misfolded state that is able to propagate by recruiting natively folded PrP. By measuring folding trajectories of single PrP molecules held under tension in a high-resolution optical trap, we found that the native folding pathway involves only two states, without evidence for partially folded intermediates that have been proposed to mediate misfolding. Instead, frequent but fleeting transitions were observed into off-pathway intermediates. Three different misfolding pathways were detected, all starting from the unfolded state. Remarkably, the misfolding rate was even higher than the rate for native folding. A mutant PrP with higher aggregation propensity showed increased occupancy of some of the misfolded states, suggesting these states may act as intermediates during aggregation. These measurements of individual misfolding trajectories demonstrate the power of single-molecule approaches for characterizing misfolding directly by mapping out nonnative folding pathways.

protein folding | optical tweezers

Protein folding involves a stochastic search through the configurational energy landscape of the protein to find the native structure. Although most proteins have evolved to fold efficiently into a unique native structure, misfolding (the formation of nonnative structures) occurs frequently in vivo (1). Cellular processes act to mitigate the effects of misfolding, e.g., by preventing misfolding from occurring with the help of molecular chaperones or by removing misfolded proteins once they have formed through the action of the proteasome (1, 2). Misfolded proteins that escape such quality-control pathways, however, can lead to a wide range of diseases, such as Alzheimer's, Parkinson's, and the prion disorders (3).

Biophysical studies of protein misfolding show that it is a very complex process (3). The many different conformations involved, the numerous alternative pathways, and the likely importance of rare or transient states all pose key technical challenges for characterizing misfolding mechanisms. Single-molecule (SM) spectroscopic approaches are well suited to overcome these challenges: Not only are they well established for studying protein folding mechanisms, but they can directly characterize distinct subpopulations, map out folding pathways, and observe rare or transient states (4). However, SM spectroscopy has not yet been widely applied to characterize protein misfolding. Misfolding has been observed in a few protein constructs using both force (5–7) and fluorescence spectroscopies (8), and the formation and growth of aggregates has been monitored with fluorescence spectroscopy (9–11), but the network of pathways available for misfolding has only begun to be mapped out in any detail (12) and not yet for any disease-related protein.

Here we describe a SM force spectroscopy study of misfolding in the prion protein PrP, a highly conserved membrane-associated protein notable for its ability to misfold into a conformation that is infectious. The infectious form, denoted PrP^{Sc}, recruits natively folded PrP, denoted PrP^{C}, to form additional PrP^{Sc}, thereby permitting transmission between individuals and species (13, 14). PrP has been studied extensively to elucidate the mechanisms for misfolding and conversion. PrP^{C} has a structured C-terminal domain containing three α-helices and two short β-strands (Fig. 1*A* and Fig. S1) and an unstructured N-terminal domain (15–17). In contrast, PrP^{Sc} is rich in β-sheets (18). Although its structure remains unknown, several models have been proposed for the amyloid fibers into which it aggregates (19–21). Infectivity is believed to arise from oligomeric PrP^{Sc} (22), with the dominant model for conversion of PrP^{C} to PrP^{Sc} involving seeded nucleation (14): Fluctuations of PrP^{C} monomers produce a rare, nonnative conformation able to form an ordered, misfolded oligomer that then recruits and stabilizes additional monomers. Partially folded intermediates of PrP have long been proposed to play a key role in this process (23), as in protein aggregation more generally (3), but evidence for their existence is conflicting: Some studies indicate only two-state folding (24), whereas others suggest the presence of an intermediate (25–28).

Despite significant advances in the characterization of PrP, misfolding and conversion still remain poorly understood, in part because they are difficult to observe directly. There have been few SM studies of prions to date: Yeast prion structural dynamics were studied with SM fluorescence (29), and the structural interactions within prion amyloid fibers were probed by force spectroscopy (30, 31), but the properties of individual molecules of PrP—especially their ability to form nonnative structures—have not yet been investigated. To observe misfolding directly in single PrP molecules, we attached kilobase-long DNA handles to the protease-resistant fragment (residues 90–231) of Syrian hamster PrP (SHaPrP), and then bound the handles specifically to polystyrene beads held in optical tweezers (Fig. 1*A*). Using the tweezers to apply denaturing tension to a single PrP molecule, we monitored the resulting dynamic structural changes in the protein by measuring the end-to-end extension of the molecule with high spatial and temporal resolution.

Author contributions: M.T.W. designed research; H.Y., X.L., K.N., and A.N.G. performed research; X.L., A.M.B., A.S., and I.S. contributed new reagents/analytic tools; H.Y. and K.N. built experimental apparatus; H.Y., X.L., and M.T.W. analyzed data; and H.Y., X.L., K.N., A.N.G., A.M.B., A.S., I.S., and M.T.W. wrote the paper.

The authors declare no conflict of interest.

This article is a PNAS Direct Submission.

[1]H.Y. and X.L. contributed equally to this work.

[2]To whom correspondence may be addressed at: National Institute for Nanotechnology, 11421 Saskatchewan Drive, Edmonton AB, T6G 2M9, Canada. E-mail: michael.woodside@nrc-cnrc.gc.ca.

This article contains supporting information online at www.pnas.org/lookup/suppl/doi:10.1073/pnas.1107736109/-/DCSupplemental.

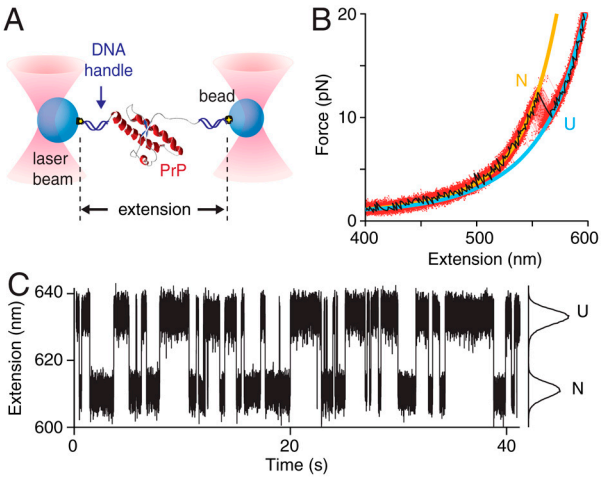

Fig. 1. Force spectroscopy measurements of PrP show apparent two-state folding. (*A*) SHaPrP(90–231) labeled at both termini with Cys residues was attached to sulfhydryl-labeled DNA strands bound to beads held in optical traps. The extension of the molecule held under tension by the traps was measured as the protein unfolded or refolded. (*B*) FECs of PrP. The handles stretch as the force rises monotonically until PrP unfolds at approximately 10 pN, causing a discrete jump in the extension and force (black). By overlaying 100 unfolding FECs (red), the contour length change is found from WLC fits to the folded (orange) and unfolded (cyan) states to be the value expected for unfolding of the native state. (*C*) With the force held constant at 9.1 pN by a passive force clamp, the extension jumps between two values corresponding to the unfolded state (U) at higher extension and natively folded state (N) at lower extension.

Results

The extension of the PrP constructs was first measured while moving the traps apart at a constant rate to ramp up the force, creating force-extension curves (FECs). The extension increased monotonically with force as the handles were stretched (Fig. 1*B*) until the protein unfolded at approximately 10 pN, causing an abrupt increase in extension and concomitant drop in force indicative of an apparently two-state process (4). Refolding curves, where the force was ramped down, also showed two-state behavior (Fig. S2). The same two-state behavior, without any distinguishable subpopulations (e.g., different contour length changes or unfolding forces), was displayed by 3,250 FECs measured on seven molecules. The contour length change, ΔL_c, determined from worm-like chain (WLC) fits to the FECs (Fig. 1*B*), was $\Delta L_c = 34.1 \pm 0.4$ nm (all uncertainties represent the standard error on the mean). The number of amino acids unfolded, n_{aa}, was calculated from $n_{aa} = (\Delta L_c + d_T)/L_c^{aa}$, where d_T is the distance between the termini of the structured domain and L_c^{aa} is the contour length per amino acid (*Supporting Information*). Given $d_T = 3.1$ nm from the NMR structure (15) and the crystallographic value $L_c^{aa} = 0.36$ nm (32), we found $n_{aa} = 103 \pm 1$, consistent with complete unfolding and refolding of the 104-aa native structure (Fig. S1).

FECs probe the folding out of equilibrium, due to the changing force. To investigate the folding under equilibrium conditions, we also measured the extension of the molecule as a function of time while the force was held constant using a passive force clamp (33). The extension jumped between two values corresponding to natively folded (N) and unfolded (U) PrP as in the FECs, spending very little time between (Fig. 1*C*). No intermediates are immediately obvious in these data, despite the proven effectiveness of constant-force measurements for detecting them (34–37). Although the observation of two-state folding agrees with some previous ensemble measurements (24), others have inferred the existence of an intermediate (25–28). To search for direct evidence of an intermediate that might be too rare or short lived to be readily apparent at first glance, we examined extensive constant-force records (several hours in total) measured at high bandwidth. A passive force clamp was essential here, to avoid artifactual transients from feedback loop closure (Fig. S3). Because these measurements were made under equilibrium conditions, the protein must have sampled all possible transitions between different conformations. Any intermediate state, I, on the native folding pathway should thus have been seen not only as a step between U and N when the molecule unfolded or refolded but also as transient excursions from U and, separately, from N (Fig. S4).

We first searched for I during the brief time spent moving between N and U. We aligned all transitions on their midpoints [Fig. 2*A* (red)] by fitting them to the logistic function (Fig. S5), and then averaged them to reduce noise: 3,364 unfolding transitions were aligned and averaged [Fig. 2*A* (black)], as were 3,318 folding transitions [Fig. 2*B* (red)]. Because an intermediate state would slow down the transition from N to U (or U to N) compared to a simple two-state process, we next compared the measured transitions to the signal produced by a single step-like motion in the trap, as would be expected for two-state folding. To do this, the motion of a reference construct containing only the DNA handles (no protein) was measured as the trap was moved abruptly (<1 μs) by 20 nm, equal to the U–N extension change. Aligning and averaging 200 such response curves as above [Fig. 2*B* (blue)], we observed that the folding and unfolding transitions [Fig. 2*B* (red and black, respectively)] have precisely the same shape as the instrument response to a step function, confirming that there is no intermediate. To determine the

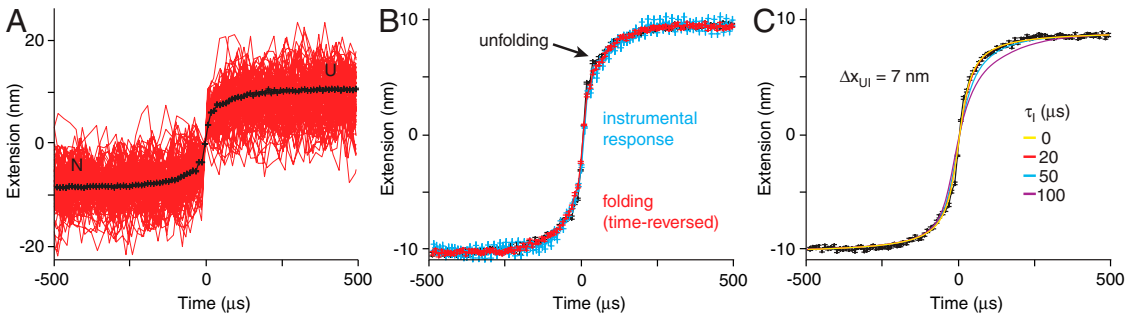

Fig. 2. On-pathway intermediates are not observed. (*A*) To search for on-pathway intermediates, 100 separate transitions between folded (N) and unfolded (U) states taken from a single constant-force record were aligned on the midpoint of the transitions (red) and averaged. The average of 3,364 transitions is shown in black. (*B*) The average of the unfolding transitions (black) and the time-reversed average of 3,318 folding transitions (red) are identical within experimental uncertainty, and the same as the average instrumental response function measured with a reference construct lacking protein (blue). An intermediate would cause the transitions to differ from the instrument response. Error bars: standard error. (*C*) The average signal expected for an obligate intermediate located 7 nm from U was simulated using the instrument response function for various lifetimes τ_I. Comparing the measured average (black) to the simulated signals (yellow red, cyan, purple: $\tau_I = 0$, 20, 50 and 100 μs, respectively) placed an upper limit of $\tau_I < 50$–100 μs for any intermediate.

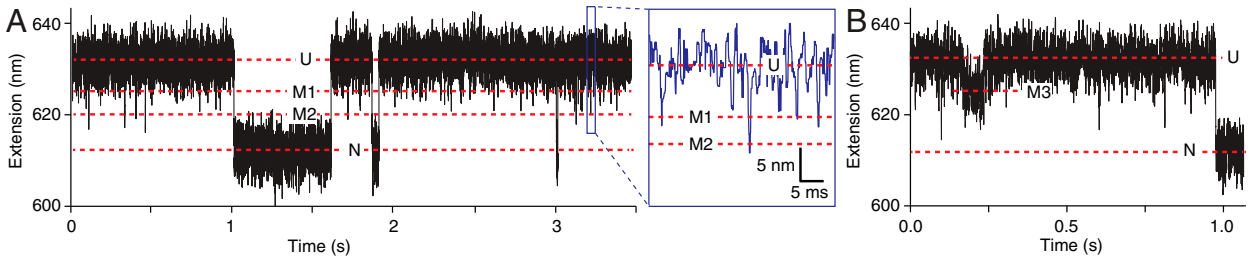

Fig. 3. Constant-force records reveal misfolded states. (*A*) High-resolution extension records at a constant force of 9.5 pN reveal frequent transient spikes down from state U, reaching two different extension values that represent off-pathway intermediates (labeled M1, M2). (*Inset*) Magnified view of data in blue square. (*B*) Transitions from U to a longer-lived off-pathway state (M3) are observed very rarely. Force = 9.2 pN.

measurement resolution and set an upper limit on the lifetime of any putative state I, τ_I, we used the transfer function describing the instrument response (Fig. S6) to simulate the shape of the average transition that would have resulted from an intermediate located at an extension Δx_{UI} from the unfolded state (Fig. S7*A*), as described in *Supporting Information*. The results are illustrated in Fig. 2*C* for $\Delta x_{UI} = 7$ nm and $\tau_I = 0$–100 μs. Multiple simulations using different Δx_{UI} and τ_I values (Fig. S7) indicate that any obligate on-pathway intermediate must have a lifetime under tension of less than approximately 50–100 μs.

We also searched for transient excursions into a possible intermediate coming from and returning to N, another type of event that must occur at equilibrium if I is on-pathway (Fig. S4). No transitions from N to any state other than U could be discerned directly from the constant-force records (Fig. 3). To determine the maximum possible occupancy of such a state consistent with our data, we measured the point-spread function (PSF) of the trap (the distribution of extensions expected due to fluctuations when measuring a fixed contour length), using the reference construct lacking protein (Fig. 4*A*). We then binned the extensions in the low-extension (nominally folded) state of the PrP trajectories and fit the resulting histogram to the PSF (Fig. 4*B*), looking for peaks corresponding to states with different extension. From the lack of peaks in the residual to these fits (Fig. S8), we estimate that any short-lived on-pathway intermediate must be occupied less than 0.001% of the time (*Supporting Information*). Because tension increases the lifetime and occupancy of extended states exponentially (38), any on-pathway intermediate would have to be exceedingly rare or short-lived at zero force.

Whereas no intermediates were observed on the native pathway, the search for rare and short-lived events did reveal several states with extensions between U and N that were only entered and exited via U and hence must be off-pathway. They were generally very short-lived (approximately 1 ms or less), appearing as "spikes" pointing down from U in the constant-force extension records (Fig. 3*A, Inset*). These spikes are not simply part of the extension distribution for U: In contrast to the native state distribution (Fig. 4*B*), a histogram of the data in the high-extension (nominally unfolded) state of the constant-force trajectory (Fig. 4*C*) reveals a small residual peak between N and U after subtracting the PSF, indicating the presence of extra states. Two additional states are needed to fit the residual: The first, M1, is located 7.1 ± 0.4 nm from U and is occupied 0.6 ± 0.1% of the time; the second, M2, is 10.5 ± 0.5 nm from U and occupied 0.11 ± 0.02% of the time. Very infrequently (approximately 6 hr^{-1}, occupancy approximately 0.04%), an additional state (denoted M3 in Fig. 3*B*) was observed 4.9 ± 0.2 nm from U, with a lifetime of approximately 50–100 ms. From the extensions and occupancies of these states at different forces (*Supporting Information*), we find that M1 has approximately 40–50 aa folded and is 3 ± 1 kcal/mol more stable than U at zero force, M2 has 60–70 aa folded and is 5 ± 2 kcal/mol more stable than U, and M3 has 30–40 aa folded and is approximately as stable as U. Because these states do not lead to the natively folded structure, they must represent misfolded conformations of PrP.

To investigate whether these nonnative states are related in some way to aggregation, we measured the folding of a mutant SHaPrP, C179A/C214A. This mutant aggregates much more readily than wild-type PrP (Fig. S9) and can form β-rich oligomers (39). Because the geometry of the SM assay isolates a single protein molecule, however, aggregation is prevented during the SM measurements, allowing us to probe how the misfolding differs in a monomer that would otherwise aggregate rapidly. FECs (Fig. S10) revealed two states with $\Delta L_c = 34 \pm 1$ nm, the value expected for the native structure, indicating that the native fold forms when the mutant is prevented from aggregating. Similar to

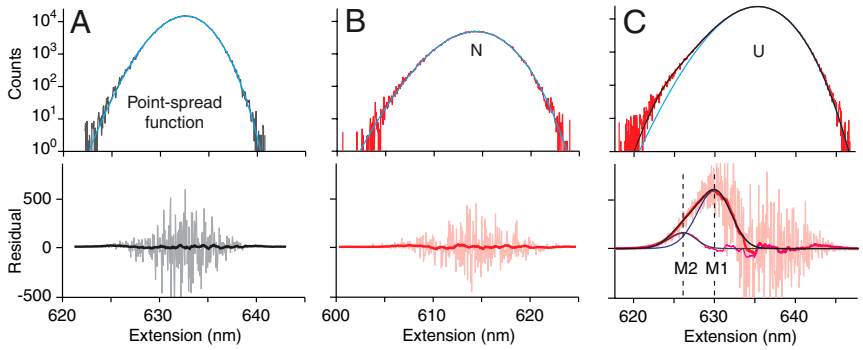

Fig. 4. Misfolded states form via the unfolded state only. (*A*) A histogram of the extension from a constant-force record of the reference construct lacking protein (*Upper*, gray) shows the PSF of the trap fit to Eq. S1 for the PSF (cyan). Counting noise in the residual (*Lower*, gray) from the histogram binning is smoothed in a 2.5-nm window (black). (*B*) A histogram of the native-state extension at constant force (*Upper*, red) fits well to the measured PSF of the trap (cyan). The residual (*Lower*, pink) is smoothed as above (red) and is featureless, showing that N does not fold/unfold into anything other than U. (*C*) Fitting the unfolded-state extension histogram (*Upper*, red) to the PSF (cyan) leaves a significant residual (*Lower*, pink). Fitting the peak in the smoothed residual (*Lower*, red) to the PSF (blue) again leaves a significant residual (purple), which is well fit by a third PSF (gray); the three PSFs together fit the full histogram completely (black). The residual fits yield the extension and occupancy of the misfolded states M1 and M2, which are entered only from U.

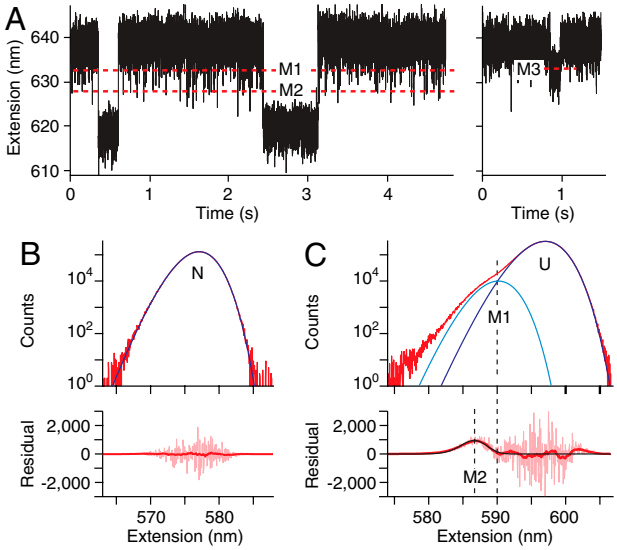

Fig. 5. Mutant PrP shows increased misfolding. (*A*) Constant-force records of the C179A/C214A mutant show transient misfolding at the same extensions as M1, M2, and M3 for wild-type PrP, with similar lifetimes. Force = 9.2 pN (*Left*), 9.7 pN (*Right*). (*B*) The native-state histogram (*Upper*, red) is well fit by the trap PSF (blue). The residual to this fit (*Lower*, pink) is featureless after smoothing (red) to remove counting noise. (*C*) The unfolded-state histogram (*Upper*, red) has a prominent shoulder. Fitting the peak and shoulder to one PSF for U (blue) and another at the location of M1 (cyan) leaves a significant peak in the smoothed residual (*Lower*, red) at the location of M2, which is well fit by a third PSF (black). M1 and M2 are several times more prevalent in the mutant than the wild-type.

the wild-type protein, misfolded states were observed in extension records at constant force (Fig. 5*A*), at the same extensions as M1–M3 and with similar kinetic properties. These states were therefore identified as states M1–M3. Notably, however, the occupancy of M1 was increased four- to fivefold and that of M2 by two- to threefold in the mutant as compared to wild-type PrP (Fig. 5 *B* and *C*), indicating that these states were, respectively, 1 and 0.5 kcal/mol more stable in the mutant (Fig. S11).

Discussion

These results offer another perspective on the complex structural dynamics of protein misfolding, through direct observation of the conformational fluctuations of single PrP molecules. The picture of the network of folding pathways that emerges for PrP (Fig. 6) reveals some surprising details that shed light on PrP misfolding. First, we find that native folding is a two-state process. We see no evidence for any partially folded intermediate on the native pathway, such as hypothesized to mediate misfolding (23), despite previous reports (25–28). We cannot completely rule out on-pathway intermediates, because force probes are not sensitive to structural changes that leave the molecular extension unchanged (as in a proposed intermediate where helix 1 restructures (40)); the chemical denaturants and low pH used in most misfolding studies might also produce intermediates not observable under

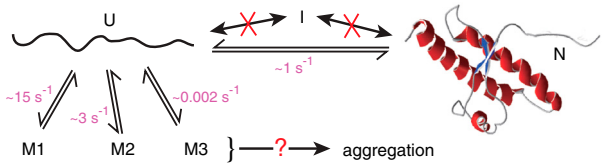

Fig. 6. Schematic diagram of folding/misfolding pathways. SHaPrP does not pass through an intermediate on the native pathway, but the unfolded state leads to three different misfolded states at varied rates. Folding and misfolding rates at approximately 9 pN are indicated. *U* = unfolded, *I* = intermediate, *N* = native, *M1–M3* = misfolded.

the conditions here. Nevertheless, partially native intermediates in which the structure changes near the termini, such as proposals with a detached β-strand 1 (41) or selectively disordered helices 2 and 3 (28), are inconsistent with our observations.

Instead of misfolding proceeding through an on-pathway intermediate, we find that nonnative structures are only accessible from the unfolded state. Indeed, there is not just one misfolding pathway but rather three of them, leading to different nonnative structures. Remarkably, PrP explores these misfolding pathways more frequently than it does the native pathway: The rates for formation of M1 and M2 estimated from the constant-force trajectories, approximately 15 s^{-1} and 3 s^{-1}, respectively (*Supporting Information*), are considerably higher than the rate for native folding at the same force, approximately 1 s^{-1}. The relative rates imply that the vast majority (>90%) of all attempts at structure formation lead to nonnative structures rather than the native state, although the resulting misfolded states are not very stable for isolated PrP molecules under these conditions and are thus rarely occupied. One type of misfolding we did not observe, however, despite the amyloid-forming propensity of residues 106–126 (42), was structure within the natively unstructured N terminus of the protein: Even transient structure formation by the N terminus while the C-terminal domain was folded would have produced a detectable peak at short extensions in the residual to the N-state extension histogram fit (Figs. 4*B* and 5*B*).

Our results suggest that the key state for misfolding may be the unfolded state (43), rather than the native state or an on-pathway intermediate. PrP could be unfolded in vivo during translocation or retro-translocation across the endoplasmic reticulum (ER) membrane (44), providing opportunities to misfold both in the ER and the cytosol. Interestingly, our measurements were made at neutral pH, similar to conditions in the cytosol, ER, and extracellular space. Previous work in vitro found that PrP does not readily misfold at neutral pH, but it does at low pH (45), supporting the hypothesis that PrP^{Sc} develops in endosomes (13). The misfolded states we found in single PrP molecules are so rarely occupied that they would be unlikely to be detected by ensemble methods, but the high misfolding rates we observe clearly indicate that PrP does indeed readily misfold at neutral pH.

The behavior of the C179A/C214A mutant provides a first look at how the observed misfolding pathways relate to aggregate formation. The β-rich oligomers that this mutant can form are similar to isoforms that have been investigated as possible intermediates for PrP^{Sc} conversion (45). The fact that the misfolded states M1 and M2 are stabilized in the mutant suggests that they could act as intermediates leading to oligomerization, with the mutation driving increased aggregation via enhanced occupancy of the misfolded intermediates. The existence of different misfolding pathways might possibly relate to the ability of PrP to form different oligomeric structures (46, 47), but additional measurements will clearly be needed to establish such a link. Additional studies will also be needed to address the question of how the misfolding of isolated PrP molecules relates to PrP^{Sc} formation, e.g., by exploring the effects of mutations enhancing pathogenicity (48), probing the effects of different pH conditions, and observing aggregate formation directly. If M1–M3 are involved, however, the need to completely unfold the native state could support models where the C-terminal domain is significantly restructured in PrP^{Sc} (19), although partially native structures (20, 21) might still form (despite being unstable in monomeric PrP) if they were stabilized during refolding into an amyloid.

A key feature of this study is the ability to observe very short-lived conformational fluctuations directly within the folding trajectories of single protein molecules, enabled by high time resolution and the capacity to resolve states with extremely low occupancies. The ability to map out the network of pathways that compete with native structure formation provides a powerful platform for investigating the molecular mechanisms of protein

misfolding. Applying this approach to other proteins involved in misfolding disorders should provide additional insight both into what features drive the unique behavior of PrP and into what commonalities exist between misfolding mechanisms for different proteins.

Methods

Sample Preparation. Truncated wild-type SHaPrP(90–232) was cloned into the pET-15b plasmid between the XhoI and EcoRI sites. N- and C-terminal Cys residues were introduced by mutating Ser residues in the thrombin cleavage site and the prion site S232, respectively. The 19-kDa, His-tagged SHaPrP was expressed in *Escherichia coli* BL21(DE3), then purified similarly to a previous protocol (49). PrP was refolded on a nickel-nitriloacetic acid column after purification, with native folding confirmed by circular dichroism spectroscopy (50). The C179A/C214A mutations were introduced by site-directed mutagenesis, and the mutant was expressed and purified similarly (39). DNA handles were attached to the protein similarly to a previous protocol (51): Refolded PrP was reduced with tris(2-carboxyethyl)phosphine (TCEP), activated with 2,2′-dithiodipyridine, then reacted with sulfhydryl-labeled DNA handles prepared by PCR (one 798 bp, labeled by biotin, the other 1,261 bp, labeled with digoxigenin). Reference constructs consisting only of the DNA handles without protein were made by creating a disulfide bond between handles.

PrP–DNA and reference constructs were incubated at approximately 100 pM with 250 pM polystyrene beads (600 nm diameter labeled with avidin, 800 nm diameter labeled with antidigoxigenin), to form dumbbells (52). Dumbbells were diluted to approximately 500 fM in 50 mM MOPS, pH 7.0, with 200 mM KCl and oxygen scavenging system (8 mU/μL glucose oxidase, 20 mU/μL catalase, 0.01% wt/vol D-glucose), before insertion into a sample cell for the optical trap.

Measurements and Analysis. Samples were measured in a custom dual-beam optical trap described previously (37). FECs were measured by moving the traps apart in 1–2 nm steps at pulling rates of 20–230 nm/s. Data were sampled at 20 kHz, filtered online with an eight-pole 10 kHz Bessel filter, and averaged over each step. Trap stiffness, calibrated as described previously (53), was 0.3 and 0.9 pN/nm. Multiple FECs from a given molecule were aligned offline to correct for instrumental drift (52). Aligned data were fit to an extensible worm-like chain model (54) parameterized by L_p (polymer persistence length), L_c (contour length), and K (elastic modulus). Two WLCs in series were used (37): one for the handles and one for the amino acids. We treated the handle L_c, L_p, and K as free parameters for fitting the folded branch of the FECs but thereafter as fixed parameters for fitting the unfolded branch. L_p and K for the unfolded amino acids were also treated as fixed parameters when fitting the unfolded branch of the FECs: $L_p = 0.65$ nm (55) and $K = 2{,}000$ pN. Hence the latter fit involved only a single free parameter, the unfolded amino acid contour length. The crystallographic contour length of an amino acid, $L_c{}^{aa} = 0.36$ nm/aa (32), was used to convert ΔL_c into n_{aa}.

Constant-force data were measured with a passive force clamp (33). Measurements were sampled at 50 kHz and filtered online with a 25 kHz eight-pole Bessel filter or sampled at 20 kHz and filtered at 10 kHz. The stiffness of the trap used to measure force was 0.3 pN/nm. Data were median-filtered offline in a 0–2 ms window depending on the application: 2 ms for separating U and N (as in Fig. 1*C*), 0.5 ms for extension histograms (as in Fig. 4), and unfiltered for measuring the transition between U and N (as in Fig. 2). Histograms were binned in 0.05 nm increments. All offline data analysis used custom software in Igor Pro (Wavemetrics).

Additional details are provided in *Supporting Information*.

ACKNOWLEDGMENTS. We thank V. Semenchenko and D. Wishart for providing cells expressing SHaPrP(90–231); D. Foster and M. Belov for assistance with instrumentation development; and members of the Woodside lab and Prion Structure & Dynamics collaboration for helpful discussions. We thank PrioNet Canada, the Alberta Prion Research Institute, the *nano*Works program of Alberta Innovates (AI), and the National Institute for Nanotechnology for financial support. X.L. and A.S. were supported by fellowships from AI Health Solutions and AI Technology Solutions, respectively.

1. Hartl FU, Hayer-Hartl M (2009) Converging concepts of protein folding in vitro and in vivo. *Nat Struct Mol Biol* 16:574–581.
2. Tyedmers J, Mogk A, Bukau B (2010) Cellular strategies for controlling protein aggregation. *Nat Rev Mol Cell Biol* 11:777–788.
3. Chiti F, Dobson CM (2006) Protein misfolding, functional amyloid, and human disease. *Annu Rev Biochem* 75:333–366.
4. Borgia A, Williams PM, Clarke J (2008) Single-molecule studies of protein folding. *Annu Rev Biochem* 77:101–125.
5. Bechtluft P, et al. (2007) Direct observation of chaperone-induced changes in a protein folding pathway. *Science* 318:1458–1461.
6. Oberhauser AF, Marszalek PE, Carrion-Vazquez M, Fernandez JM (1999) Single protein misfolding events captured by atomic force microscopy. *Nat Struct Biol* 6:1025–1028.
7. Yu J, Malkova S, Lyubchenko YL (2008) Alpha-Synuclein misfolding: Single molecule AFM force spectroscopy study. *J Mol Biol* 384:992–1001.
8. Borgia MB, et al. (2011) Single-molecule fluorescence reveals sequence-specific misfolding in multidomain proteins. *Nature* 474:662–665.
9. Hillger F, Nettels D, Dorsch S, Schuler B (2007) Detection and analysis of protein aggregation with confocal single molecule fluorescence spectroscopy. *J Fluoresc* 17:759–765.
10. Nath S, Meuvis J, Hendrix J, Carl SA, Engelborghs Y (2010) Early aggregation steps in alpha-synuclein as measured by FCS and FRET: Evidence for a contagious conformational change. *Biophys J* 98:1302–1311.
11. Orte A, et al. (2008) Direct characterization of amyloidogenic oligomers by single-molecule fluorescence. *Proc Natl Acad Sci USA* 105:14424–14429.
12. Stigler J, Ziegler F, Gieseke A, Gebhardt JC, Rief M (2011) The complex folding network of single calmodulin molecules. *Science* 334:512–516.
13. Caughey B, Baron GS, Chesebro B, Jeffrey M (2009) Getting a grip on prions: Oligomers, amyloids, and pathological membrane interactions. *Annu Rev Biochem* 78:177–204.
14. Cobb NJ, Surewicz WK (2009) Prion diseases and their biochemical mechanisms. *Biochemistry* 48:2574–2585.
15. James TL, et al. (1997) Solution structure of a 142-residue recombinant prion protein corresponding to the infectious fragment of the scrapie isoform. *Proc Natl Acad Sci USA* 94:10086–10091.
16. Lysek DA, et al. (2005) Prion protein NMR structures of cats, dogs, pigs, and sheep. *Proc Natl Acad Sci USA* 102:640–645.
17. Zahn R, et al. (2000) NMR solution structure of the human prion protein. *Proc Natl Acad Sci USA* 97:145–150.
18. Pan KM, et al. (1993) Conversion of alpha-helices into beta-sheets features in the formation of the scrapie prion proteins. *Proc Natl Acad Sci USA* 90:10962–10966.
19. Cobb NJ, Sonnichsen FD, McHaourab H, Surewicz WK (2007) Molecular architecture of human prion protein amyloid: A parallel, in-register beta-structure. *Proc Natl Acad Sci USA* 104:18946–18951.
20. DeMarco ML, Daggett V (2004) From conversion to aggregation: Protofibril formation of the prion protein. *Proc Natl Acad Sci USA* 101:2293–2298.
21. Govaerts C, Wille H, Prusiner SB, Cohen FE (2004) Evidence for assembly of prions with left-handed beta-helices into trimers. *Proc Natl Acad Sci USA* 101:8342–8347.
22. Silveira JR, et al. (2005) The most infectious prion protein particles. *Nature* 437:257–261.
23. Cohen FE, et al. (1994) Structural clues to prion replication. *Science* 264:530–531.
24. Wildegger G, Liemann S, Glockshuber R (1999) Extremely rapid folding of the C-terminal domain of the prion protein without kinetic intermediates. *Nat Struct Biol* 6:550–553.
25. Apetri AC, Maki K, Roder H, Surewicz WK (2006) Early intermediate in human prion protein folding as evidenced by ultrarapid mixing experiments. *J Am Chem Soc* 128:11673–11678.
26. Hart T, et al. (2009) Folding kinetics of the human prion protein probed by temperature jump. *Proc Natl Acad Sci USA* 106:5651–5656.
27. Jenkins DC, Sylvester ID, Pinheiro TJ (2008) The elusive intermediate on the folding pathway of the prion protein. *FEBS J* 275:1323–1335.
28. Kuwata K, et al. (2002) Locally disordered conformer of the hamster prion protein: A crucial intermediate to PrPSc? *Biochemistry* 41:12277–12283.
29. Mukhopadhyay S, Krishnan R, Lemke EA, Lindquist S, Deniz AA (2007) A natively unfolded yeast prion monomer adopts an ensemble of collapsed and rapidly fluctuating structures. *Proc Natl Acad Sci USA* 104:2649–2654.
30. Dong J, Castro CE, Boyce MC, Lang MJ, Lindquist S (2010) Optical trapping with high forces reveals unexpected behaviors of prion fibrils. *Nat Struct Mol Biol* 17:1422–1430.
31. Ganchev DN, Cobb NJ, Surewicz K, Surewicz WK (2008) Nanomechanical properties of human prion protein amyloid as probed by force spectroscopy. *Biophys J* 95:2909–2915.
32. Pauling L, Corey RB (1951) The pleated sheet, a new layer configuration of polypeptide chains. *Proc Natl Acad Sci USA* 37:251–256.
33. Greenleaf WJ, Woodside MT, Abbondanzieri EA, Block SM (2005) Passive all-optical force clamp for high-resolution laser trapping. *Phys Rev Lett* 95:208102.
34. Cecconi C, Shank EA, Bustamante C, Marqusee S (2005) Direct observation of the three-state folding of a single protein molecule. *Science* 309:2057–2060.
35. Gebhardt JC, Bornschlogl T, Rief M (2010) Full distance-resolved folding energy landscape of one single protein molecule. *Proc Natl Acad Sci USA* 107:2013–2018.
36. Woodside MT, et al. (2006) Direct measurement of the full, sequence-dependent folding landscape of a nucleic acid. *Science* 314:1001–1004.
37. Neupane K, Yu H, Foster DAN, Wang F, Woodside MT (2011) Single-molecule force spectroscopy of the add adenine riboswitch relates folding to regulatory mechanism. *Nucleic Acids Res* 39:7677–7687.
38. Bustamante C, Chemla YR, Forde NR, Izhaky D (2004) Mechanical processes in biochemistry. *Annu Rev Biochem* 73:705–748.
39. Maiti NR, Surewicz WK (2001) The role of disulfide bridge in the folding and stability of the recombinant human prion protein. *J Biol Chem* 276:2427–2431.
40. De Simone A, Zagari A, Derreumaux P (2007) Structural and hydration properties of the partially unfolded states of the prion protein. *Biophys J* 93:1284–1292.

41. Hosszu LL, et al. (2005) Definable equilibrium states in the folding of human prion protein. *Biochemistry* 44:16649–16657.
42. Kuwata K, et al. (2003) NMR-detected hydrogen exchange and molecular dynamics simulations provide structural insight into fibril formation of prion protein fragment 106–126. *Proc Natl Acad Sci USA* 100:14790–14795.
43. Hosszu LL, et al. (1999) Structural mobility of the human prion protein probed by backbone hydrogen exchange. *Nat Struct Biol* 6:740–743.
44. Ma J, Wollmann R, Lindquist S (2002) Neurotoxicity and neurodegeneration when PrP accumulates in the cytosol. *Science* 298:1781–1785.
45. Bjorndahl TC, et al. (2011) Detailed biophysical characterization of the acid-induced PrP(c) to PrP(beta) conversion process. *Biochemistry* 50:1162–1173.
46. Chakroun N, et al. (2010) The oligomerization properties of prion protein are restricted to the H2H3 domain. *FASEB J* 24:3222–3231.
47. Gerber R, Tahiri-Alaoui A, Hore PJ, James W (2007) Oligomerization of the human prion protein proceeds via a molten globule intermediate. *J Biol Chem* 282:6300–6307.
48. van der Kamp MW, Daggett V (2009) The consequences of pathogenic mutations to the human prion protein. *Protein Eng Des Sel* 22:461–468.
49. Zahn R, von Schroetter C, Wuthrich K (1997) Human prion proteins expressed in *Escherichia coli* and purified by high-affinity column refolding. *FEBS Lett* 417:400–404.
50. Stockel J, Safar J, Wallace AC, Cohen FE, Prusiner SB (1998) Prion protein selectively binds copper(II) ions. *Biochemistry* 37:7185–7193.
51. Cecconi C, Shank EA, Dahlquist FW, Marqusee S, Bustamante C (2008) Protein-DNA chimeras for single molecule mechanical folding studies with the optical tweezers. *Eur Biophys J* 37:729–738.
52. Greenleaf WJ, Frieda KL, Foster DA, Woodside MT, Block SM (2008) Direct observation of hierarchical folding in single riboswitch aptamers. *Science* 319:630–633.
53. Neuman KC, Block SM (2004) Optical trapping. *Rev Sci Instrum* 75:2787–2809.
54. Wang MD, Yin H, Landick R, Gelles J, Block SM (1997) Stretching DNA with optical tweezers. *Biophys J* 72:1335–1346.
55. Shank EA, Cecconi C, Dill JW, Marqusee S, Bustamante C (2010) The folding cooperativity of a protein is controlled by its chain topology. *Nature* 465:637–640.

Supporting Information

Yu et al. 10.1073/pnas.1107736109

SI Text

Protein-DNA Construct Design. The amino acid sequence of the recombinant SHaPrP(90–231) protein and corresponding structural and functional elements are displayed in Fig. S1. We note that recombinant SHaPrP(90–231) is able to form PrP^{Sc} in vitro (1).

Protein Purification. After expression, cell pellets were resuspended in buffer A (6M GnHCl, 10 mM Tris, 100 mM NaH_2PO_4, 10 mM reduced glutathione, pH 8.0) and sonicated for 2 min. The lysate was centrifuged, filtered, and then purified by FPLC (GE Healthcare) using a Ni-NTA column. After rinsing the protein bound to the column with buffer A, PrP was refolded on the column using gradient exchange from buffer A to buffer B (10 mM Tris, 100 mM NaH_2PO_4, pH 8.0). Impurities were removed by rinsing on column with buffer C (10 mM Tris, 100 mM NaH_2PO_4, 50 mM imidazole, pH 8.0). The refolded PrP was then eluted with buffer D (10 mM Tris, 100 mM NaH_2PO_4, 500 mM imidazole, pH 5.8), before dialysis into 50 mM sodium phosphate buffer, pH 7.0. Product purity and identity were assessed by SDS/PAGE and Western blotting (Antiprion(109–112) clone 3F4, Millipore).

DNA Handle Attachment. The refolded protein was first reduced with tris(2-carboxyethyl)phosphine (TCEP) in a 100:1 molar ratio with PrP for 30 min. It was then desalted by spin column (Zeba, Thermo Scientific) to remove excess TCEP and activated with 2,2′-dithiodipyridine (Sigma-Aldrich). The CD spectrum of the activated protein confirmed that it remained in the native fold. The activated protein was next reacted with sulfhydryl-labeled DNA handles of two different lengths prepared by PCR. One handle was 798-bp long and labeled at opposite termini by sulfhydryl and biotin, the other 1,261-bp long and terminally labeled with sulfhydryl and digoxigenin. The formation of the correct construct length was verified by gel electrophoresis.

Optical Trap Instrumentation. Two orthogonally polarized laser beams from the same 5W 1,064-nm laser (Spectra-Physics) were used to generate two traps. The position of each trap was controlled independently by one acousto-optic deflector (AOD, AA Optoelectronique) and one electro-optic deflector (EOD, Conoptics) in each axis. The traps were moved apart during all measurements using the EODs only. The stiffness of each trap was controlled by the AODs. Bead positions within the traps were measured by collecting the light from two orthogonally polarized beams at 633 nm scattered by the beads onto independent position-sensitive diodes (Pacific Silicon Sensors). Trap automation and data collection used custom Labview software (National Instruments).

Force-Extension Curves (FECs) of PrP Compared to Reference Construct. Individual FEC measurements of the PrP construct are shown in Fig. S2 for unfolding of PrP (red), where the force on the protein is ramped up until it unfolds, and refolding of the same molecule (blue), where the force on the protein is ramped back down until the protein refolds. The folding transition is seen as a sudden jump in extension and force as the extension of the molecule changes. For comparison, a FEC measurement (black) of the reference construct containing no protein, only DNA handles, shows just the worm-like chain (WLC) elasticity of DNA, without any unfolding features.

FEC Analysis of Contour Length. To determine the change in contour length (ΔL_c) upon unfolding and refolding, the aligned FECs were fit to an extensible WLC model (2):

$$F(x) = \frac{k_B T}{L_p}\left[\frac{1}{4}\left(1 - \frac{x}{L_c} + \frac{F}{K}\right)^{-2} - \frac{1}{4} + \frac{x}{L_c} - \frac{F}{K}\right],$$

where L_p is the persistence length of the polymer, L_c is the contour length, K is the elastic modulus, and k_B is the Boltzmann constant. The crystallographic contour length of an amino acid, $L_c{}^{aa} = 0.36$ nm/aa (3), was used to convert ΔL_c into the number of amino acids unfolded (n_{aa}), rather than the slightly larger value reported from high-force pulling experiments using an atomic force microscope (4), according to the equation $n_{aa} = (\Delta L_c + \Delta d_T)/L_c{}^{aa}$. Here we explicitly included the term Δd_T to take into account the fact that as the structure changes, the distance between the two termini of the structured parts of the protein (the points at which force is instantaneously being applied) changes, too. In the case of the unfolded state, $d_T = 0$, whereas for the native state, $d_T = 3.1$ nm is determined from the NMR structure of the protein (5).

Constant-Force Measurements. Constant force was verified during passive force clamp measurements using the force recorded in the harmonic trap, as described previously (6). As shown in Fig. S3, the force did not jump between two different levels as would be expected if the force were changing between the folded and unfolded states (7); instead, only fluctuations were observed. Importantly, no transients were observed in the force, as always occur during measurements using a force clamp based on an active feedback loop (8). To demonstrate that the force is truly constant, the force measured simultaneously with the extension record (Fig. S3*A*) was partitioned into two subsets corresponding to the time spent respectively in the folded (blue) and unfolded (red) states, as determined from the extension record. Histograms of these two subsets of the force record display Gaussian behavior, with the centers differing by less than 0.07 pN (Fig. S3*B*).

Alignment of Folding and Unfolding Transitions at Constant Force. To search for short-lived intermediate states within the transition from N to U (or U to N), multiple transitions were aligned and averaged to reduce the effects of Brownian motion and determine the shape (extension vs. time) of the folding and unfolding transitions accurately. The transitions were aligned by fitting each transition to the logistic function, an analytic approximation to the Heaviside step function that matches the shape of the transition reasonably well:

$$X(t) = \frac{1}{1 + \exp[-\alpha(t - t_0)]}, \qquad \textbf{[S1]}$$

where X is the end-to-end extension, t_0 is the time at the center of the transition, and α represents the slope of the transition (as $\alpha \to \infty$, $X(t) \to \Theta(t)$, the Heaviside step function). The records were aligned on the t_0 fit values for each transition (Fig. S5).

A total of 3,364 folding transitions recorded from different molecules at a variety of forces (within approximately 1 pN of the force at which PrP was poised equally between U and N) were aligned this way, as were 3,318 unfolding transitions. All folding transitions were then averaged, as were the unfolding transitions. No asymmetry was observed between the shapes of the average folding and unfolding transitions: The time-reversed unfolding

curve matches the folding curve within experimental uncertainty (Fig. 2*B*).

Instrumental Response Function. The response of the optical trap to a step function signal [Fig. S6 (blue)] was determined using a reference construct containing no protein, just the DNA handles attached together via disulfide bonds. The reference construct was held between the traps, the traps were moved suddenly (<1 μs), and the resulting motion of the reference construct was measured with the detectors. Such measurements reflect the intrinsic filtering effects of all aspects of the instrumentation (including the effects of the beads and handles); they can be used to determine the effective transfer function that smoothes the actual extension change in the protein according to $O(t) = X(t) \otimes H(t)$, where $O(t)$ is the observed extension record, $X(t)$ is the actual extension time series of the protein itself, and $H(t)$ is the transfer function of the instrument. 200 measurements of the response of the optical trap detectors were averaged as described above for the unfolding/refolding transitions. The amplitude of the trap motion was made equal to the extension change between U and N at constant force (20 nm). Approximating the fast impulse used to measure the response as a true step function, the response is described well if the transfer function is Lorentzian [Fig. S6 (red)].

Modeling the Effect of an Intermediate State. To model the shape of the folding transition expected at constant force if an obligate intermediate I were present, we generated waveforms containing step functions from U to I and then from I to N. Step functions were used as an approximation for the fast (μs-scale) transition time for protein folding (9), which is much faster than the time response of the optical trap (approximately 100 μs, see Fig. S6). The lifetime in state I was chosen randomly from an exponential distribution with mean value τ. Two hundred such curves were generated, convolved with the Lorentzian transfer function to match the shape that would be expected in the measurement (illustrated in Fig. S7*A*) and then averaged as for the experimentally measured transitions. This procedure simulated the average transition that would be measured for a given value of intermediate lifetime τ and extension change between U and I, Δx_{UI}.

Fig. 2*C* compares simulations with $\Delta x_{UI} = 7$ nm (the extension change from U to M1) and $\tau = 0$, 20, 50, and 100 μs (respectively yellow, red, cyan, purple) to the experimental data (black). Fig. S7*B* repeats the calculation with $\Delta x_{UI} = 10.0$ nm (the extension change from U to M2) and the same lifetimes. The experimental data are clearly inconsistent with an obligate intermediate having Δx_{UI} close to these values unless the intermediate lifetime is less than approximately 50–100 μs, thereby ruling out the possibility that M1 and M2 (which have longer lifetimes) might be on the native folding pathway.

Finally, Fig. S7 *C* and *D* repeat the same calculations, this time simulating what would be expected for an on-pathway intermediate close to the native state, such as would occur if β-strand 1 were to detach (10). If all the N-terminal residues up to E146 were detached in state I (i.e., everything up to helix 1), then the expected extension change between N and I, Δx_{NI}, would be $\Delta x_{NI} = 4.5$ nm; if only the residues up to R136 detached, then it would be $\Delta x_{NI} = 2.3$ nm. The area around position 139 is known from NMR experiments on bovine PrP to be relatively stable to chemical denaturation (11). Simulations with $\tau = 0$, 20, 50, 100, and 150 μs (respectively yellow, red, cyan, purple, and green) in Fig. S7 *C* and *D* show that the experimental data are inconsistent with such an intermediate unless its lifetime is less than approximately 100 μs.

Optical Trap Point Spread Function. To determine the point spread function (PSF) of the optical trap for extension measurements, i.e., the distribution of extensions that would be expected for a construct of fixed length, we measured extension records for the reference constructs described above (DNA handles attached together without any protein between them). These reference constructs were identical to the PrP constructs except that they lacked PrP. Extension records measured at constant force with a 50 kHz bandwidth for approximately 100 s displayed distributions that were almost Gaussian but partly asymmetric (Fig. 4*A*).

For a harmonic potential with fixed stiffness, the PSF should be Gaussian (7, 12). The asymmetry we observe is due to the anharmonicity of the trapping potential used for the passive force clamp (6): The amplitude of the Brownian fluctuations in the position of the bead is here sufficiently large that the bead explores a significant portion of the anharmonic portion of the potential well. The trap stiffness experienced by this bead therefore varies across the distribution of bead positions. At high displacements from the trap center (corresponding to low molecular extensions) the bead visits regions of negative stiffness, thereby decreasing the effective stiffness of the system (traps plus molecule), whereas at low displacements (corresponding to high molecular extensions) the bead visits regions of positive stiffness, increasing the effective system stiffness. The low-extension side of the Gaussian distribution expected for a harmonic trap is therefore stretched out, whereas the high-extension side is compressed.

These effects were modeled phenomenologically by describing the PSF as a Gaussian-like function with an extension-dependent width parameter:

$$P(x) = \begin{cases} A \exp\left[-\frac{(x-x_0)^2}{2(\sigma - c|x-x_0|)^2}\right], & x > x_0 \\ A \exp\left[-\frac{(x-x_0)^2}{2(\sigma + c|x-x_0|)^2}\right], & x < x_0. \end{cases} \quad \textbf{[S2]}$$

Here c represents the extension-dependent stretching or compression of the distribution width, and σ represents the extension-independent component of the width. This function fits the data very well, leaving effectively no residual other than counting noise (Fig. 4*A*).

Fitting Histograms to the PSF. The coefficients c and σ for the PSF [Eq. **S2**] were determined empirically from measurements of the reference compound and thereafter treated as fixed parameters when fitting the PrP extension histograms as in Fig. 4. To average over statistical counting noise, the residuals from fits of the histograms (as in Figs. 4 and 5) were smoothed with a boxcar filter using a 2.5 nm window. This window was smaller than the half-width of the PSF (approximately 3 nm) and hence would not obscure true signals.

Analysis of On-Pathway Intermediates and Limits of Detection. An intermediate state I on the pathway from U to N might be obligate (e.g., if there is only one pathway from U to N) or nonobligate (e.g., if there is more than one pathway from U to N), as illustrated in Fig. S4*A*. Regardless of the nature of the intermediate, in measurements where the system is in thermodynamic equilibrium (such as constant-force records of long duration), all possible pathways between accessible states must be sampled. Hence any on-pathway state I must in general be observed in three ways: (i) as a "step" between U and N as the molecule folds or unfolds; (ii) as a "spike" up from N, when N unfolds transiently into I and then refolds; and (iii) as a spike down from U, when U folds transiently into I that then unfolds again.

An example of this behavior is seen when measuring the extension at constant force (Fig. S4*B*) of a simple DNA hairpin with a sequence designed to generate an obligate intermediate in force-spectroscopy measurements (13). The intermediate is clearly seen as a step between U and N, as a spike up from N, and as a spike down from U. Such results are qualitatively different from the PrP measurements shown in Figs. 1 and 3.

The failure to observe any steps between U and N, whether directly in the records or indirectly via the average of the protein folding/unfolding transitions (as described above), indicates that an obligate on-pathway intermediate does not exist, unless its lifetime is less than the time resolution of the measurements (estimated from the simulations above at approximately 50–100 μs). Even an intermediate located as little as 2 nm from U or N is ruled out. A rare, nonobligate intermediate is more difficult to rule out by observing the transitions between N and U: Its effects might be lost when averaging the transitions because they are overwhelmed by the transitions containing no intermediate. However, this would only be true if the intermediate lifetime is short compared to the averaging window needed to reduce the Brownian noise significantly. For example, states with lifetimes approximately 0.5 ms or greater can be readily observed directly from extension records filtered at 0.5 ms. In particular, states M1 and M2 (with lifetimes estimated at approximately 0.3–0.5 ms) are clearly detected in the records displayed in Fig. 1*C* and Fig. 3*A*.

To place an upper bound on the occurrence of any rare, nonobligate intermediate, we analyzed the behavior in state N. First, we examined the constant-force records for spikes indicating transient unfolding from N to I, especially for evidence of a state I that is well separated from N in distance and has a lifetime of approximately 0.5 ms or longer. Considering transient unfolding from N to I with Δx_{NI} approximately 10 nm or more (i.e., a large extension change), we saw no evidence for such transitions at the level of one event per 300 s (upper bound based on the typical minimum record length), leading to an estimate of approximately 0.0002% for the maximum occupancy of such a state.

Because this analysis would not reveal states with very short lifetimes, especially if they involve only a small distance change, we next examined the histograms of the extension values recorded when the protein was nominally in state N. Any partially unfolded intermediate with a different extension than N would show up as an extra peak in the histogram, due to transitions from N to I and back. After fitting the extension histograms in state N to the PSF (as in Fig. 2*C*), no peaks were observed in the residuals with $\Delta x_{\mathrm{NI}} < 10$ nm having an area greater than approximately 0.01% of the total histogram area. The small peaks that did remain in the residual were almost certainly noise, as their location changed from one histogram to the next (Fig. S8*A*). Averaging over all the residuals to look for any peak occurring consistently at any given extension, we obtain the estimate of approximately 0.001% for the maximum occupancy of a nonobligate intermediate.

Misfolded State Fit Residuals. The quality of the fits for states M1 and M2 is demonstrated by the small residuals left after fitting the high-extension data in the constant-force trajectories (i.e., the nominally unfolded state) to the PSFs for U, M1, and M2 (Fig. S8*B*).

Folding Rate Estimations. The average folding rate from U to N was measured directly from the extension records. The average folding rate from U to M3 was also estimated directly from the extension records. However, transitions into states M1 and M2 were difficult to identify directly from the extension records, as they were both very short-lived and had low occupancy. We therefore estimated the folding rates for M1 and M2 by dividing the total time spent in each state (determined from the area of the fits to the extension histograms as in Fig. 4*C*) by the lifetime of the states estimated from the extension records (as in Fig. 3*A, Inset*) to determine the number of transitions into M1 or M2, and then dividing the total time spent in the unfolded state by the number of transitions. The average lifetimes were estimated as being approximately 0.3–0.5 ms for both states. Given the average occupancies for M1 and M2 (0.6% and 0.1%, respectively), this resulted in rates of approximately 15 s^{-1} and approximately 3 s^{-1}, respectively.

FECs of the C179A/C214A Mutant. FEC measurements of the C179A/C214A mutant (2,410 curves from three molecules) were used to determine the contour length change from folded to unfolded (Fig. S10). Fits to the extensible WLC model as described for the wild-type protein yielded $\Delta L_c = 34 \pm 1$ nm, the same value as for wild-type PrP. If the mutant had formed a nonnative fold, we would expect to observe a different length change. The excellent agreement with ΔL_c expected for the native structure (34.3 nm) indicates that the mutant forms the same fold as wild-type PrP in these measurements.

Aggregation of the C179A/C214A Mutant Compared to Wild-Type PrP. We monitored the aggregation of C179/A C214/A PrP and wild-type PrP using a turbidity assay, similar to a previously published method (14). Briefly, 40 μM protein in 10 mM phosphate buffer (pH 7.0) was incubated for a week at 37 °C while being agitated at 300 rpm, and the turbidity was measured periodically using a microplate reader via the optical density at 420 nm. The mutant aggregated during sample preparation before the first turbidity measurement was made [Fig. S9 (red)]. The same turbidity was observed with and without reducing agent present (4 mM TCEP). Wild-type PrP aggregated more slowly: When reduced with TCEP, aggregation occurred over the course of 1 d, but without TCEP the protein was stable for more than 1 wk [Fig. S9 (blue)].

Disulfide Bond. Wild-type SHaPrP has a disulfide bond between C179 and C214 (5). This bond is present in our protein samples after purification and refolding, as shown by a Raman peak at 533 cm^{-1} that is in the 510–540 cm^{-1} range specific to S-S bonds (15). However, we observe no signature of the disulfide bond in the force-spectroscopy measurements: The full contour length of the structured domain unfolds in a single step at a force much lower than typically needed to break disulfide bonds, without any intermediate state at the distance expected from the NMR structure for unfolding everything up to the disulfide (22.2 nm). It therefore seems unlikely that the disulfide is present during the force-spectroscopy measurements. It is possible the bond does not re-form properly after reduction to attach the DNA handles, or it might be broken while handling the beads at the outset of the measurement, when very large but uncalibrated forces are typically applied. The oxygen-scavenging system that protects against oxidative damage of the protein and DNA creates a nonoxidizing environment, reducing the likelihood of re-forming a disulfide bond.

Free Energy of Misfolded States. Equilibrium measurements allow the free energy differences between states to be determined directly from the ratio of occupancies of the states, using the Boltzmann probability (16):

$$\ln(P_M/P_U) = -k_{\mathrm{B}}T(\Delta G_{\mathrm{fold}} + \Delta G_{\mathrm{stretch}} - F \cdot \Delta x_{MU}), \quad \textbf{[S3]}$$

where P_M is the probability of finding state M, P_U is the probability of finding state U, k_{B} is the Boltzmann constant, ΔG_{fold} is the folding equilibrium free energy of M relative to U, $\Delta G_{\mathrm{stretch}}$ is the free energy required to stretch out the unfolded amino acids under tension, F is the applied tension, and Δx_{MU} is the extension change between M and U. P_M/P_U was obtained from the extension histograms and plotted as a function of force for each misfolded state (Fig. S11). The plot was then fitted to Eq. **S3**, treating Δx_{MU} as a fixed parameter whose value was determined from the extension histograms. The stretching energy, estimated from the WLC model, was then subtracted from the zero-force intercept of the fit to obtain the folding energy of the misfolded state at zero force.

1. Kim JI, et al. (2010) Mammalian prions generated from bacterially expressed prion protein in the absence of any mammalian cofactors. *J Biol Chem* 285:14083–14087.
2. Wang MD, Yin H, Landick R, Gelles J, Block SM (1997) Stretching DNA with optical tweezers. *Biophys J* 72:1335–1346.
3. Pauling L, Corey RB (1951) The pleated sheet, a new layer configuration of polypeptide chains. *Proc Natl Acad Sci USA* 37:251–256.
4. Ainavarapu SR, et al. (2007) Contour length and refolding rate of a small protein controlled by engineered disulfide bonds. *Biophys J* 92:225–233.
5. James TL, et al. (1997) Solution structure of a 142-residue recombinant prion protein corresponding to the infectious fragment of the scrapie isoform. *Proc Natl Acad Sci USA* 94:10086–10091.
6. Greenleaf WJ, Woodside MT, Abbondanzieri EA, Block SM (2005) Passive all-optical force clamp for high-resolution laser trapping. *Phys Rev Lett* 95:208102.
7. Gebhardt JC, Bornschlogl T, Rief M (2010) Full distance-resolved folding energy landscape of one single protein molecule. *Proc Natl Acad Sci USA* 107:2013–2018.
8. Fernandez JM, Li H (2004) Force-clamp spectroscopy monitors the folding trajectory of a single protein. *Science* 303:1674–1678.
9. Shaw DE, et al. (2010) Atomic-level characterization of the structural dynamics of proteins. *Science* 330:341–346.
10. Hosszu LL, et al. (2005) Definable equilibrium states in the folding of human prion protein. *Biochemistry* 44:16649–16657.
11. Julien O, Chatterjee S, Thiessen A, Graether SP, Sykes BD (2009) Differential stability of the bovine prion protein upon urea unfolding. *Protein Sci* 18:2172–2182.
12. Woodside MT, et al. (2006) Direct measurement of the full, sequence-dependent folding landscape of a nucleic acid. *Science* 314:1001–1004.
13. Woodside MT, Garcia-Garcia C, Block SM (2008) Folding and unfolding single RNA molecules under tension. *Curr Opin Chem Biol* 12:640–646.
14. Frankenfield KN, Powers ET, Kelly JW (2005) Influence of the N-terminal domain on the aggregation properties of the prion protein. *Protein Sci* 14:2154–2166.
15. Spiro TG, Gaber BP (1977) Laser Raman scattering as a probe of protein structure. *Annu Rev Biochem* 46:553–572.
16. Bustamante C, Chemla YR, Forde NR, Izhaky D (2004) Mechanical processes in biochemistry. *Annu Rev Biochem* 73:705–748.

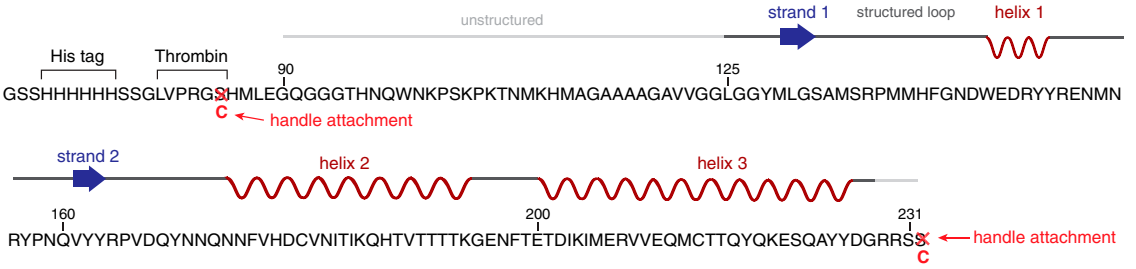

Fig. S1. Sequence and secondary structure of SHaPrP(90–231) construct. The secondary structure and key functional areas (e.g., His tag, Cys residues for DNA handle attachments) are annotated on the amino acid sequence.

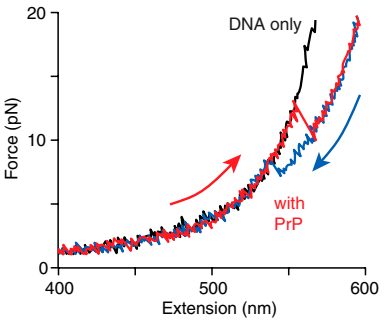

Fig. S2. Unfolding and refolding FECs of PrP compared to reference construct without protein. The unfolding FEC of PrP (red) and refolding FEC (blue) both contain a single sawtooth feature demonstrating two-state behavior. Because the two curves overlap before and after the folding transition, the contour length change is the same in each case. For comparison, a FEC for the reference construct lacking protein (black) demonstrates only the WLC elasticity of the DNA handles, without any unfolding transition.

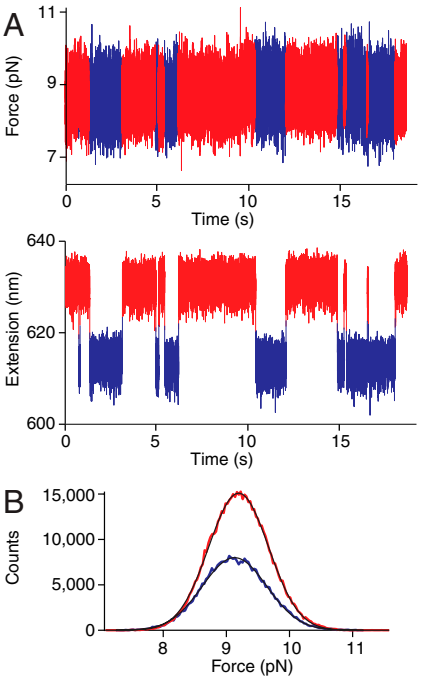

Fig. S3. Force remains constant during constant-force measurements. (*A*) Force and extension records measured simultaneously using the passive force clamp. The force remains unchanged whether the protein is folded (blue) or unfolded (red); no transients are observed as the folding/unfolding takes place. (*B*) Histograms of the force in the folded (blue) and unfolded (red) states are well fit by Gaussians whose peaks differ by only 0.07 pN.

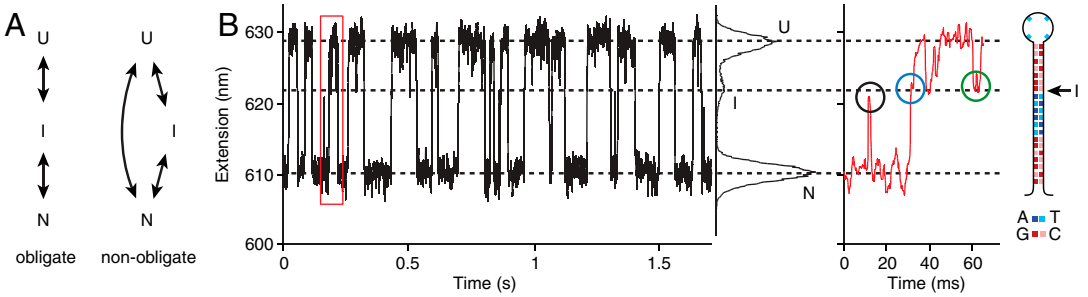

Fig. S4. Signature of an intermediate state in constant-force measurements. (*A*) An intermediate state (I) on the native folding pathway could be obligate, if there is only one pathway from unfolded (U) to native (N) (*Left*), or nonobligate, if there is more than one pathway from U to N (*Right*). (*B*) Constant-force measurement of a DNA hairpin with a stem sequence designed to produce a single obligate intermediate at the location marked by the arrow. An intermediate is clearly seen in the extension histogram. It is also seen directly in the extension record: as transient spikes from N to I (black circle) and from U to I (green circle), as well as in the form of brief steps during the motion between N and U (blue circle). The red box represents the area displayed with an expanded timescale.

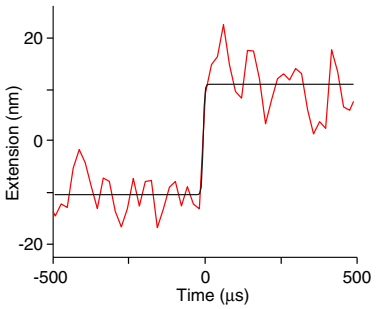

Fig. S5. Fitting the folding/unfolding transitions at constant force. The extension recorded during a single unfolding transition (red) at constant force, as in Fig. 3*A*, is fit by Eqn **S1** (gray).

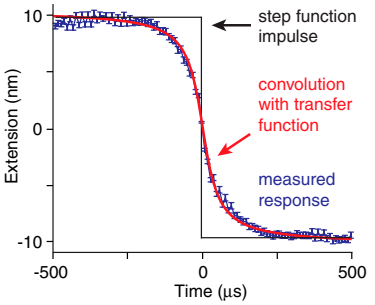

Fig. S6. Instrument response function. The average instrument response (blue) to a step impulse function (black) is well-approximated by the convolution of the impulse function with a Lorentzian transfer function (red).

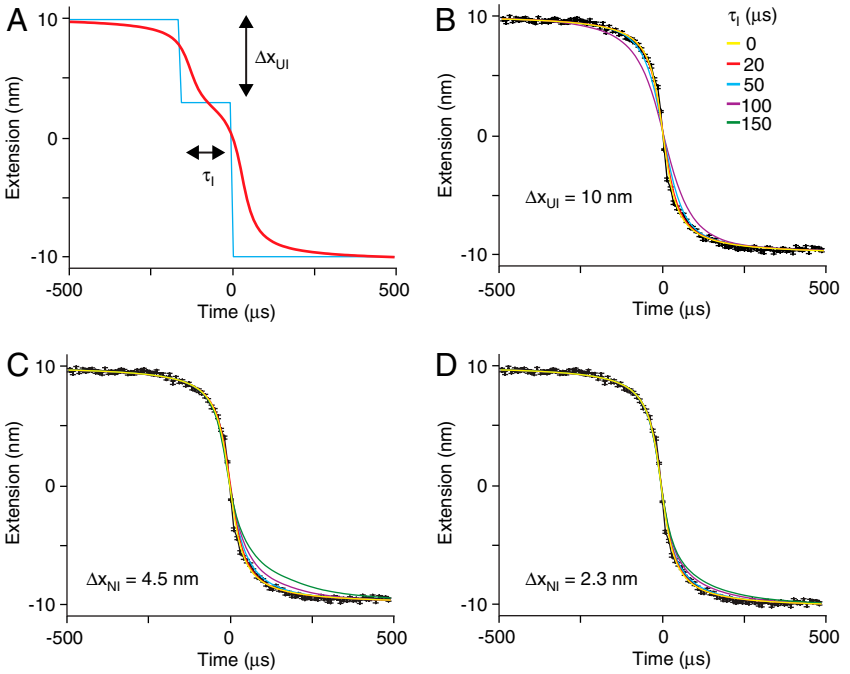

Fig. S7. Simulation of intermediate states. (*A*) A step function from U to I and then from I to N was generated to simulate the presence of an intermediate a distance Δx_{UI} from U (cyan). This was convolved with the Lorentzian transfer function to add in the filtering effect of the instrument (red), and then averaged for exponentially distributed lifetimes with mean value τ_I. (*B*)-(*D*)Simulated transitions involving obligate intermediate states with varying lifetimes τ, located 10 nm from U (*B*), 4.5 nm from N (*C*), and 2.3 nm from N (*D*), respectively. Black: average measured transition; yellow, red, cyan, purple, green: simulated transitions with $\tau = 0$, 20, 50, 100, and 150 μs respectively.

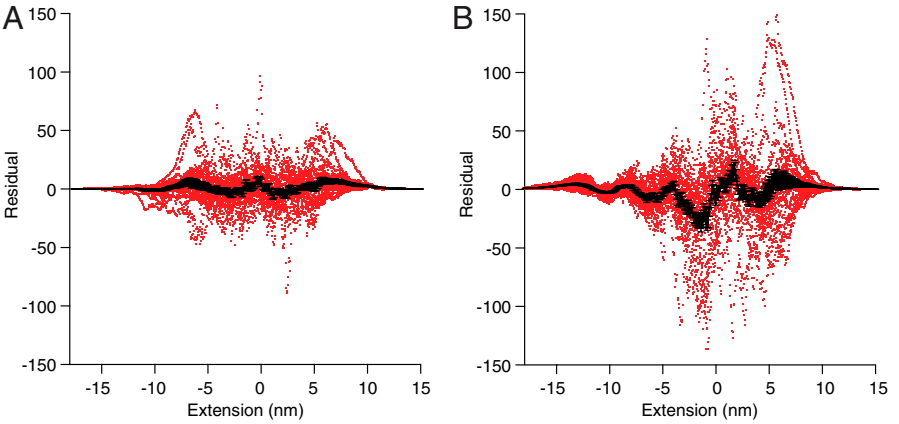

Fig. S8. Residuals for extension histogram fits. (*A*) The residuals from fitting the low-extension peak of the extension histograms (N in Fig. 1*C*) to the PSF of the trap, as in Fig. 4*B*, are shown for 22 constant-force records (red) containing over 29 million data points in total. All residuals were aligned on the peak of the original histogram. The amplitudes and locations of any peaks in the residuals fluctuate randomly. The average of all aligned residuals (black) is featureless, indicating that there is no other state present. Error bars indicate standard error on the mean. (*B*) The residuals from fitting the high-extension peak of the extension histograms (as in Fig. 4*C*) to PSFs for states U, M1, and M2 are shown for 22 constant-force records (red) containing over 86 million data points in total. Again, the average (black) is featureless, indicating the excellence of the fits.

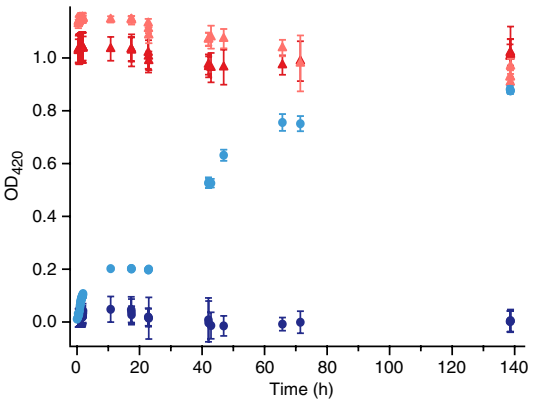

Fig. S9. Aggregation of wild-type and C179A/C214A PrP. Turbidity measurements indicate that the C179A/C214A mutant aggregates very rapidly at pH 7, during sample preparation, whether oxidized (dark red) or reduced by TCEP (light red). In contrast, wild-type PrP aggregates at pH 7 over the course of a day when reduced (light blue) but does not aggregate over at least a week when not reduced (dark blue). Error bars represent the standard error on the mean of the optical density measured in three wells.

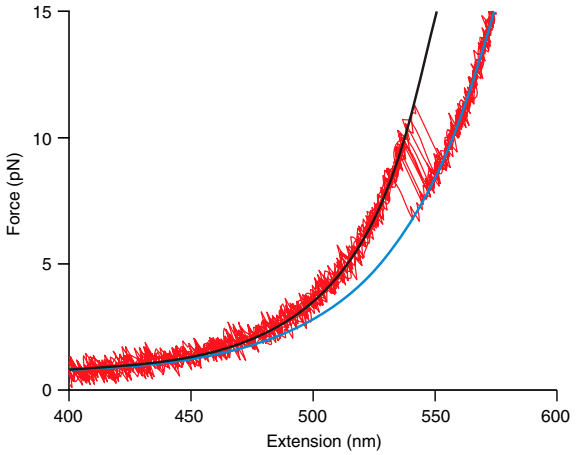

Fig. S10. FECs of C179A/C214A mutant. Ten unfolding FECs (red) measured on the C179A/C214A mutant show two-state unfolding. WLC fits to the folded (black) and unfolded (blue) states reveal a contour length change of 34 ± 1 nm, the result expected for unfolding of the native structure (34.3 nm).

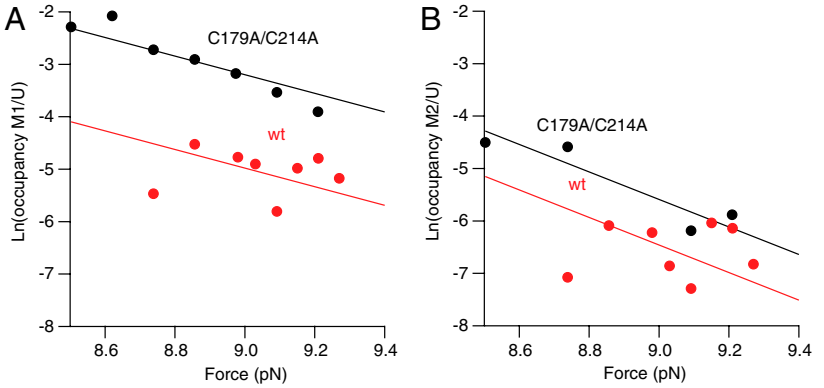

Fig. S11. Free energy of the misfolded states. The misfolded:unfolded occupancy ratio for states M1 (*A*) and M2 (*B*) as a function of force were used to determine the misfolding free energies from fits to Eq. **S3**, for both wild-type PrP (red) and the C179A/C214A mutant (black). The slope of the fit, which is set by the extension change during misfolding, was treated as a fixed parameter determined from the extension histograms.